Decomposition mechanism of methylamine to hydrogen cyanide on Pt(111): Selectivity of the C–H, N–H and C–N bond scissions

ARTICLE *in* RSC ADVANCES · JANUARY 2014

Impact Factor: 3.84 · DOI: 10.1039/c3ra46544f

8 AUTHORS, INCLUDING:

Daniel Deng
City University of Hong Kong
32 PUBLICATIONS **22** CITATIONS
SEE PROFILE

Dongliang Jin
China University of Petroleum
8 PUBLICATIONS **16** CITATIONS
SEE PROFILE

Xiaofan Shi
China University of Petroleum
29 PUBLICATIONS **17** CITATIONS
SEE PROFILE

RSC Advances

PAPER

Decomposition mechanism of methylamine to hydrogen cyanide on Pt(111): selectivity of the C–H, N–H and C–N bond scissions†

Cite this: *RSC Adv.*, 2014, **4**, 12266

Zhigang Deng, Xiaoqing Lu,* Zengqiang Wen, Shuxian Wei, Qing Zhu, Dongliang Jin, Xiaofan Shi and Wenyue Guo*

Received 10th November 2013
Accepted 3rd January 2014

DOI: 10.1039/c3ra46544f

www.rsc.org/advances

Periodic density functional theory (DFT) calculations were performed to systematically investigate the decomposition mechanism of methylamine (CH_3NH_2) to hydrogen cyanide (HCN) on Pt(111). The geometries and energies for all species involved are analyzed, and the decomposition network is mapped out to elaborate the reaction mechanism. Our results show that the CH_3NH_2, methanimine (CH_2NH) and HCN prefer to desorb, while the other species prefer to decompose; the decomposition pathway prefers the successive N–H bond scissions followed by the C–H bond scissions, that is, $CH_3NH_2 \rightarrow CH_3NH \rightarrow CH_3N \rightarrow CH_2N \rightarrow HCN$. The electronic structure and energy barrier analysis are used to identify the initial competitive scissions of C–H, N–H and C–N bonds. The interaction between fragments and surface in the TS plays a decisive role in controlling the energy barrier of initial CH_3NH_2 decomposition on Pt(111). Finally, the Brønsted–Evans–Polanyi (BEP) relation identifies that the C–H and N–H bond scissions stay competitive, but the C–N bond scission is not facile to occur.

Introduction

Amines are extraordinary materials widely involved in biological systems, surface physical chemistry and environmental science.[1–3] Among them, methylamine (CH_3NH_2) is the simplest aliphatic amine containing a C–N single bond, and regarded a research prototype for more complicated amine.[4] Moreover, CH_3NH_2 is the precursor in the industrial synthesis of HCN by the Andrussow process,[5–7] along the following pathway at non-oxidative condition (known as the Degussa process):[6]

$$CH_4 + NH_3 \xrightarrow{-H_2} CH_3NH_2 \xrightarrow{-H_2} CH_2NH \xrightarrow{-H_2} HCN \quad (1)$$

Therefore, investigating the interaction between CH_3NH_2 and metal surfaces is important to understand the fundamental reactions of aliphatic amines and metal surfaces, and to design an efficient catalyst for conversion of CH_3NH_2 in the Andrussow process.

An abundance of experimental studies have focused on CH_3NH_2 adsorption and decomposition on transition metal surfaces, such as Ni,[1,8–10] Pt,[2,11–14] Rh,[4,15] Pd,[16] Cr,[1] Cu,[17] W,[18] Mo[19] and Ru.[20] Most of these results have pointed out that CH_3NH_2 is bonded to metal surfaces through the lone pair of the N atom. Although there is a variety of catalysts and reaction conditions, the decomposition of CH_3NH_2 would start with one of the N–H, C–H and C–N bond scissions, and usually gives rise to HCN, H_2, C_2N_2 and/or even C and N_2.[11,15,16] By virtue of electron energy loss spectroscopy (EELS), Baca *et al.*[1] found that CH_3NH_2 was adsorbed molecularly on Ni(100), Ni(111), Cr(100), and Cr(111) at 300 K and the C–N bond scission occurred on Cr surfaces but not on Ni. Using X-ray photoelectron spectrometry (XPS), secondary ion mass spectrometry (SIMS) and thermal desorption spectrometry (TDS), Chen *et al.*[16] found that CH_3NH_2 underwent only a dehydrogenation reaction on Pd(111), and the surface intermediates of CH_3NH, CH_2N, HCN and CN were identified without the C–N bond activation species. On Pt(111), Bridge *et al.*[11] using angle resolved ultraviolet photoemission spectroscopy (ARUPS) and TDS, reported that CH_3NH_2 dehydrogenation started with the N–H bond scission and finally produced H_2, HCN and C_2N_2, while the C–N bond scission path yielded N_2 and hydrocarbons. The dehydrogenation reaction pathway was speculated to occur along $CH_3NH_2 \rightarrow CH_3NH \rightarrow CH_2N \rightarrow HCN$; however, employing temperature programmed desorption (TPD) and auger electron spectroscopy (AES), Hwang *et al.*[2] found that CH_3NH_2 dehydrogenated totally and a HCN product was formed only from dehydrogenations, and that no C–N bond scission existed at 600 K. Obviously, experimental investigations provided massive amounts of information on the catalytic reactions of CH_3NH_2. However, experimental evidence for detailed catalytic mechanisms, such as bond activation of the C–H, N–H and C–N bond, selectivity and sequence of bond

College of Science, China University of Petroleum, Qingdao, 266580, P. R. China. E-mail: luxq@upc.edu.cn; wyguo@upc.edu.cn; Fax: +86 532 8698 3363; Tel: +86 532 8698 1334

† Electronic supplementary information (ESI) available: The coverage effect test, the metastable adsorption configurations, and decomposition of CH_2NH_2 and HCN are presented. See DOI: 10.1039/c3ra46544f

scission, elementary reaction steps, and competitive reaction channels *etc.*, have not been convincingly elucidated.

Theoretical investigations are of great help for understanding the reaction mechanisms, especially for DFT investigations applied to reveal the microscopic adsorption structures, decomposition configurations, reaction pathways, and reaction kinetics and thermodynamics.[21–23] Lv *et al.*[24] carried out DFT modelling to understand the initial CH_3NH_2 decomposition on Ni(111) and Ni(100), and found that CH_3NH_2 scission sequence took place with the order of C–H > N–H > C–N. Moreover, they investigated CH_3NH_2 decomposition on Mo(100)[25,26] and Pd(111),[27] and the results showed that the most likely decomposition pathway was $CH_3NH_2 \rightarrow CH_2NH_2 \rightarrow CHNH_2 \rightarrow CNH_2 \rightarrow C + NH_2$ on Mo(100) and $CH_3NH_2 \rightarrow CH_2NH_2 \rightarrow CHNH_2 + CH_2NH \rightarrow CNH_2 + HCNH \rightarrow CNH + HCN$ on Pd(111). Oliva *et al.* investigated HCN hydrogenation to CH_3NH_2 on Ni(111)[28] and Co(111),[29] and found that the reaction mechanism of the hydrogenation pathway on both surfaces was $HCN \rightarrow CNH_2 + HCNH \rightarrow CH_2NH \rightarrow CH_2NH_2 + CH_2NH \rightarrow CH_3NH_2$. Platinum is an effective catalyst for the Andrussow and Degussa processes,[5,30,31] and the Pt(111) surface is often considered because this most stable surface dominates in small particles used in catalysts.[32] However, there is no deep theoretical work relevant to the CH_3NH_2 decomposition on Pt surface. In this work, we performed periodic DFT investigations on the adsorption configurations, elementary reaction processes, reaction network, potential energy surfaces, and energy barrier analysis to elucidate CH_3NH_2 decomposition on Pt(111), highlighting the competitive nature of C–H, N–H and C–N bond scissions of species derived CH_3NH_2 decomposition.

Computational details

All calculations were performed in the frame of DFT with the program package DMol^3 at the Materials Studio of Accelrys Inc.,[33–35] using the exchange–correlation functional of GGA-PW91 approximation.[36–38] To take the relativity effect into account, the density functional semicore pseudopotential (DSPP)[39] method was employed. Localized double-numerical basis sets were chosen together with polarization functions (DNP). A Fermi smearing of 0.005 Hartree and a real-space cutoff of 4.5 Å were used to improve the computational performance. The Pt(111) surface was modeled by a four-layer slab with four platinum atoms per layer representing a $p(2 \times 2)$ unit cell. Periodic images of the slab were separated by a 12 Å vacuum gap. The reciprocal space was sampled with a $(5 \times 5 \times 1)$ k-point grid generated automatically using the Monkhorst–Pack method.[40] Full-geometry optimization was performed for all relevant adsorbates and the uppermost two layers without symmetry restriction, while the bottom layer Pt atoms were fixed at the bulk-truncated positions at the experimentally determined lattice constant of 2.775 Å. Besides, the coverage effect was evaluated and no obvious influence was observed (see Fig. S1 and Table S1 in the ESI†).

The adsorption energy (E_{ads}) of an adsorbate on Pt(111) was calculated using the formula:

$$E_{ads} = E_{gas} + E_{Pt} - E_{gas/Pt} \quad (2)$$

where E_{gas} is the energy of the gas-phase species, E_{Pt} is the energy of the clean Pt(111) surface and $E_{gas/Pt}$ is the total energy of the adsorbate on Pt(111). By this definition, positive E_{ads} implies stable adsorption.

Transition state (TS) searches were performed at the same theoretical level with the complete Linear synchronous transit/quadratic synchronous transit (LST/QST) method implemented in DMol^3.[41] We applied the TS theory formalism to predict the rate constants for all the elementary steps involved. The rate constant k and pre-exponential A^0 were estimated using the conventional TS theory:[42]

$$k = \frac{k_B T}{\hbar} \frac{Q_{TS}}{Q_{IS}} \exp\left(\frac{-E_a}{RT}\right) = A^0 \exp\left(\frac{-E_a^0}{RT}\right) \quad (3)$$

where k_B is the Boltzmann constant, R is the gas constant, $\hbar$ is Planck's constant, T is the temperature following experimental conditions for Pt-based catalysts (300 K);[4] E_a^0 and E_a are energy barriers with and without zero point energy (ZPE) corrections. Q_{IS} and Q_{TS} are the partition functions at the IS and TS, respectively.

Result and discussion

In order to clarify the reaction of CH_3NH_2 decomposing to HCN on the Pt(111) surface, we first describe the adsorption structures of the relevant species, then we discuss all possible elementary reaction steps in detail.

Adsorption

In this section, we present detailed investigation on the intermediates involved in CH_3NH_2 decomposition on Pt(111). Table 1 lists the adsorption energies of the diversity of adsorption configurations. Fig. 1 presents the stable structures, while the metastable structures are given in Fig. S2 (see ESI†).

CH_3NH_2 binds weakly to the Pt surface *via* the lone pair electron of the N atom at the top site with η^1(N) configuration, corresponding to an adsorption energy of 0.99 eV. The C–N, N–H and C–H bond lengths of adsorbed CH_3NH_2 are 1.485, 1.023–1.024 and 1.097–1.098 Å, close to the corresponding gas-phase values of 1.472, 1.018 and 1.099–1.101 Å, respectively. This indicates that there is no significant activation of CH_3NH_2 when adsorbed on Pt(111), similar to previous DFT studies about CH_3NH_2 absorbed on Ni(100) and Ni(111).[24] CH_2NH_2 prefers to absorb at the bridge site with η^1(N)–η^1(C) configuration, in which both CH_2 and NH_2 fragments locate at the top sites. The corresponding adsorption energy is 2.35 eV, and the C–N bond length is 1.480 Å with the C–N axis almost parallel to the surface. The C atom is closer to the surface Pt atom than N atom (2.073 *vs.* 2.179 Å). For CH_3NH, the bridge-η^2(N) is the most stable configuration with an absorption energy of 2.18 eV. The C–N bond length of the adsorbed CH_3NH is 1.468 Å and the two N–Pt bonds are 2.115 and 2.117 Å. These results are very similar to previous DFT studies about CH_2NH_2 and CH_3NH on Pd(111).[27] All of the CH_2NH, CH_3N and CH_2N species prefer to locate at the fcc sites with the η^2(N)–η^1(C), η^3(N) and η^2(N)–η^1(C) configurations, and the corresponding absorption energies are

Table 1 Adsorption configurations, adsorption energies (in eV), and structural parameters (in angstroms) for intermediates involved in CH_3NH_2 decomposing to HCN on Pt(111)

Species	Configuration[a]	E_{ads}	d_{C-N}	d_{C-H}	d_{N-H}	d_{X-Pt}
CH_3NH_2	top-η^1(N)	0.99	1.485	1.097, 1.097, 1.098	1.023, 1.024	2.191[b]
CH_2NH_2	top-η^1(N)	2.28	1.399	1.094, 1.094	1.020, 1.020	2.138[b]
	bridge-η^1(N)–η^1(C)	2.35	1.480	1.095, 1.095	1.022, 1.021	2.179,[b] 2.073[c]
CH_3NH	top-η^1(N)	1.78	1.451	1.108, 1.103, 1.097	1.025	2.020[b]
	bridge-η^2(N)	2.18	1.468	1.101, 1.100, 1.097	1.024	2.115,[b] 2.117[b]
CH_2NH	top-η^1(N)	0.92	1.282	1.095, 1.092	1.025	2.057[b]
	fcc-η^2(N)–η^1(C)	1.10	1.447	1.098, 1.098	1.024	2.112,[b] 2.108,[b] 2.067[c]
	hcp-η^2(N)–η^1(C)	0.99	1.449	1.098, 1.098	1.024	2.114,[b] 2.113,[b] 2.069[c]
CH_3N	fcc-η^3(N)	3.38	1.451	1.098, 1.098, 1.098		2.028,[b] 2.028,[b] 2.027[b]
	hcp-η^3(N)	3.02	1.451	1.098, 1.098, 1.098		2.038,[b] 2.033,[b] 2.033[b]
CH_2N	top-η^1(N)	1.60	1.264	1.107, 1.102		2.005[b]
	bridge-η^2(N)	1.85	1.272	1.095, 1.095		2.041,[b] 2.042[b]
	fcc-η^2(N)–η^1(C)	1.91	1.382	1.098, 1.098		2.065,[b] 2.061,[b] 2.144[c]
	hcp-η^2(N)–η^1(C)	1.76	1.388	1.097, 1.097		2.071,[b] 2.064,[b] 2.152[c]
HCNH	bridge-η^1(N)–η^1(C)	2.97	1.290	1.097	1.021	2.082,[b] 1.972[c]
	fcc-η^1(N)–η^2(C)	2.85	1.329	1.097	1.021	2.062,[b] 2.237,[c] 2.059[c]
	hcp-η^1(N)–η^2(C)	2.77	1.331	1.097	1.021	2.062,[b] 2.233,[c] 2.064[c]
HCN	top-η^1(N)	0.38	1.160	1.075		2.016[b]
	bridge-η^1(N)–η^1(C)	0.91	1.249	1.096		2.064,[b] 2.046[c]
CH_3	top-η^1(C)	2.20		1.095, 1.095, 1.096		2.075[c]
CH_2	bridge-η^2(C)	4.14		1.095, 1.096		2.063,[c] 2.060[c]
CH	fcc-η^3(C)	6.46		1.095		2.016,[c] 2.011,[c] 2.010[c]
	hcp-η^3(C)	6.33		1.094		2.013,[c] 2.010,[c] 2.010[c]
NH_2	top-η^1(N)	2.10			1.027, 1.027	2.020[b]
	bridge-η^2(N)	2.51			1.021, 1.021	2.015,[b] 2.013[b]
NH	fcc-η^3(N)	3.89			1.023	2.017,[b] 2.015,[b] 2.015[b]
	hcp-η^3(N)	3.52			1.023	2.025,[b] 2.022,[b] 2.021[b]
N	fcc-η^3(N)	4.37				1.980,[b] 1.981,[b] 1.983[b]
	hcp-η^3(N)	4.12				1.986,[b] 1.992,[b] 1.992[b]
H	top-η^1(H)	2.85				1.555[d]
	bridge-η^2(H)	2.70				1.779,[d] 1.746[d]
	fcc-η^3(H)	2.70				1.991,[d] 1.832,[d] 1.820[d]
	hcp-η^3(H)	2.66				1.901,[d] 1.898,[d] 1.840[d]

[a] Top, bridge, fcc and hcp are adsorption site, η^n(X) denotes that X atom interacts with n surface metal atoms. [b] N–Pt bond length. [c] C–Pt bond length. [d] H–Pt bond length.

1.10, 3.38 and 1.91 eV, respectively. The C–N axis of CH_3N at the most stable configuration is almost perpendicular to the surface with a bond length of 1.451 Å. Analogously, both HCNH and HCN favor locating at the bridge site with η^1(N)–η^1(C) configurations, and the corresponding absorption energies are 2.97 and 0.91 eV. The C–N axis in the most stable absorbed HCNH and HCN configurations is parallel to the surface, and their bond lengths are 1.290 and 1.249 Å, respectively.

CH_3 adsorbs at the top site through the C atom, the C–Pt distance is 2.075 Å, and the C–H bond lengths are in the range of 1.095–1.096 Å. This configuration accounts for an adsorption energy of 2.20 eV. CH_2 is stably adsorbed at the bridge site, as mirrored by the adsorption energy of 4.14 eV. This configuration favours a tetrahedral configuration, in which two C–Pt bonds are calculated to be 2.060 and 2.063 Å. CH prefers to locate upright at the fcc site *via* the C end on Pt(111), and the relevant adsorption energy is 6.46 eV. The C–Pt bonds are 2.010–2.016 Å and the C–H bond is 1.095 Å. Those results are quite similar to our previous DFT studies of CH_x (x = 1–3) on Pt(111).[32] NH_2 prefers to locate at the bridge site in C_{2v} symmetry with an adsorption energy of 2.51 eV. Structurally, the two equal N–H bonds are 1.021 Å and the two N–Pt bonds are 2.013 and 2.015 Å. NH is in favour of the fcc site with a binding energy of 3.89 eV. The N–H bond is 1.023 Å and the N–Pt bond lengths range from 2.015 to 2.017 Å. For absorbed N, the most stable site is fcc and the adsorption energy is 4.37 eV. It tends to form a sp^3 hybrid configuration, in which N is almost tetrahedral, and the N–Pt bonds are 1.980–1.983 Å. Those are similar to previous DFT studies about NH_x (x = 0–2) on Pt(111).[43] For H, the binding energies at the top, bridge, fcc and hcp sites are very close (see Table 1), in agreement with the DFT result of H on Pt(111).[32,44] Notably, such close difference between the various adsorption geometries can lead to the H atoms diffusion freely on Pt(111).

Decomposition reaction pathways

In this section, the main decomposition pathways of CH_3NH_2 to HCN on Pt(111) *via* C–H, N–H and C–N bond scissions are discussed. The thermodynamic and kinetic parameters of all elementary steps are summarized in Table 2. The corresponding TS structures for each reaction are shown in Fig. 2. The reaction networks of CH_3NH_2 decomposition on Pt(111) are presented in Fig. 3.

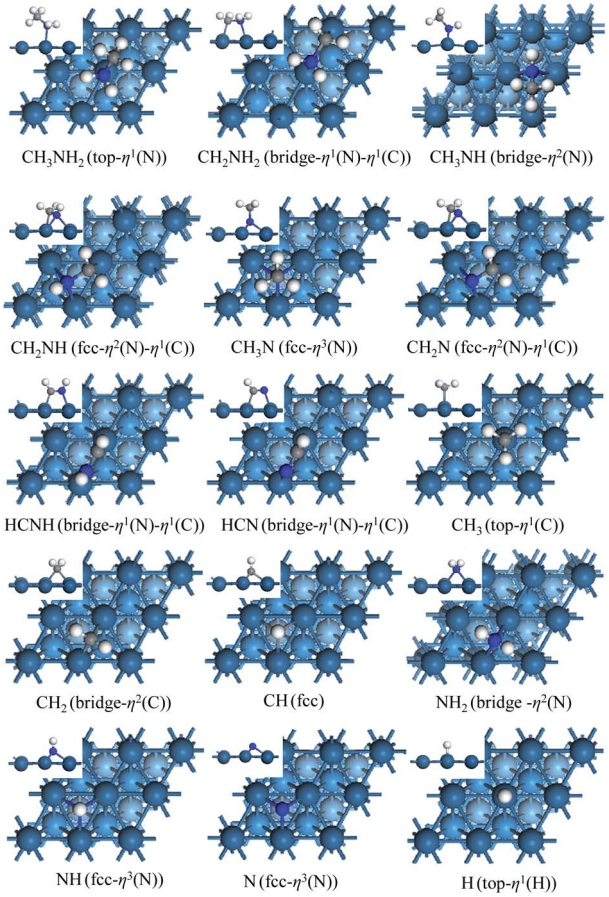

Fig. 1 The most stable adsorption configurations of intermediates involved in methylamine decomposing to HCN on Pt(111).

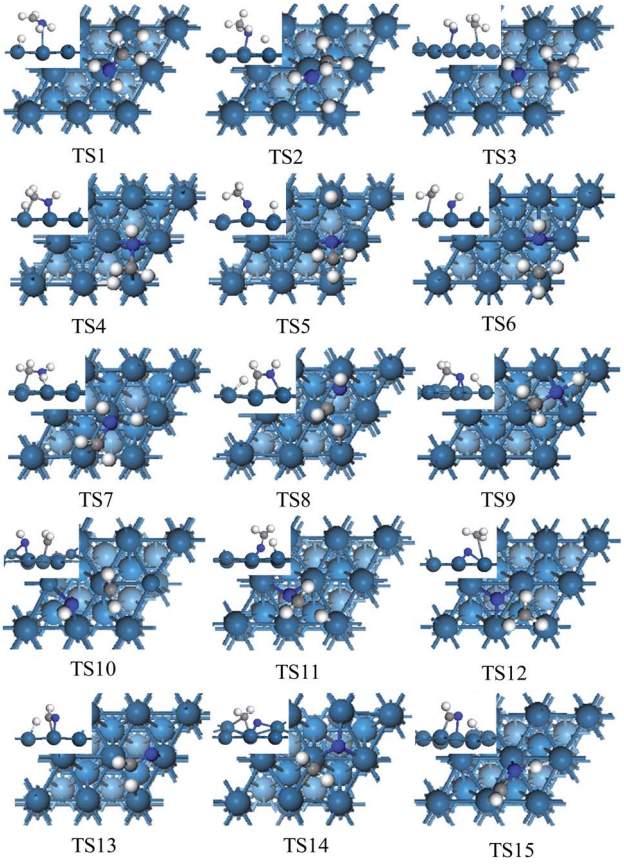

Fig. 2 TS structures of the elementary reactions involved in methylamine decomposing to HCN on Pt(111).

CH_3NH_2 decomposition. It can be envisioned that initial CH_3NH_2 decomposition may take place *via* three possible pathways, that is, the initial C–H, N–H and C–N bond scissions. To determine which bond is easier to cleave, we calculate the thermodynamic and kinetic parameters of these three elementary reactions.

$CH_3NH_2 \rightarrow CH_2NH_2 + H$. For the initial C–H bond scission, the H atom is stripped from CH_3NH_2, which locates originally at the top site with η^1(N) configuration and forms CH_2NH_2 at the bridge site and H at the top site. In the TS1, CH_2NH_2 locates at

Table 2 Reaction energies ΔE, energy barriers E_a (in eV), pre-exponential factors A^0 and rate constants k (in s^{-1}) at 300 K for the elementary steps involved in methylamine to HCN on Pt(111)

Reactions	ΔE	E_a	E_a^0	d	A^0	k
(a) $CH_3NH_2 \rightarrow CH_2NH_2 + H$	0.11	1.30	1.06	2.532^a	6.15×10^{17}	9.59×10^{-1}
(b) $CH_3NH_2 \rightarrow CH_3NH + H$	0.95	1.05	0.89	1.967^b	9.91×10^{14}	1.11×10^{0}
(c) $CH_3NH_2 \rightarrow CH_3 + NH_2$	0.67	2.38	2.23	2.112^c	1.41×10^{15}	5.76×10^{-23}
(d) $CH_3NH \rightarrow CH_2NH + H$	0.21	1.28	1.10	1.516^a	5.09×10^{15}	1.98×10^{-3}
(e) $CH_3NH \rightarrow CH_3N + H$	1.09	1.19	1.05	2.526^b	1.00×10^{15}	2.27×10^{-3}
(f) $CH_3NH \rightarrow CH_3 + NH$	0.19	2.27	2.12	2.116^c	2.42×10^{15}	6.42×10^{-21}
(g) $CH_2NH_2 \rightarrow CH_2NH + H$	0.77	1.27	1.03	1.533^b	4.72×10^{16}	2.49×10^{-1}
(h) $CH_2NH \rightarrow CHNH + H$	0.04	1.31	1.09	1.435^a	7.04×10^{16}	4.17×10^{-2}
(i) $CH_2NH \rightarrow CH_2N + H$	0.66	1.38	1.17	1.408^b	2.26×10^{16}	4.96×10^{-4}
(j) $CH_2NH \rightarrow CH_2 + NH$	0.94	2.47	2.35	2.287^c	1.06×10^{15}	3.43×10^{-25}
(k) $CH_3N \rightarrow CH_2N + H$	0.62	1.71	1.49	1.683^b	2.05×10^{16}	1.76×10^{-9}
(l) $CH_3N \rightarrow CH_3 + N$	0.69	2.64	2.50	2.395^c	6.58×10^{15}	7.13×10^{-27}
(m) $CH_2N \rightarrow HCN + H$	−0.11	0.82	0.64	1.255^a	9.38×10^{15}	2.01×10^{5}
(n) $CH_2N \rightarrow CH_2 + N$	1.10	2.04	1.98	1.938^c	5.34×10^{13}	3.08×10^{-20}
(o) $HCNH \rightarrow HCN + H$	0.65	1.52	1.24	1.346^b	8.33×10^{17}	2.72×10^{-8}

[a] Distance of C–H that break in a reaction. [b] Distance of N–H that break in a reaction. [c] Distance of C–N that break in a reaction.

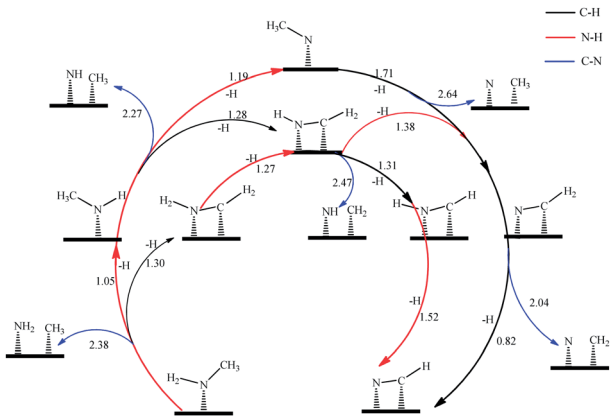

Fig. 3 Reaction network and reaction energy barriers not including ZPE correction (in eV) for methylamine decomposing to HCN on Pt(111).

the top site and H at the bridge site, and the N–Pt and C–H distances are elongated to 2.901 and 2.532 Å, respectively. The energy barrier is calculated to be 1.30 eV, and the reaction energy is slightly endothermic by 0.11 eV.

$CH_3NH_2 \rightarrow CH_3NH + H$. The initial N–H bond scission starts with CH_3NH_2 at the top site, ends with CH_3NH at the bridge site and H at the top site. In the TS2, CH_3NH remains at the top site and the H atom tilts toward the top site. The N–H distance is elongated to 1.967 Å from 1.023 Å in the IS. The reaction energy for this step is highly endothermic by 0.95 eV with an energy barrier of 1.05 eV.

$CH_3NH_2 \rightarrow CH_3 + NH_2$. The C–N bond scission is facilitated by the stretching vibration of $CH_3\cdots NH_2$. In TS3, both CH_3 and NH_2 entities are adsorbed on the neighboring top sites with a C–N distance of 2.112 Å. Finally, the C–N bond cleaves to form CH_3 at the top site and NH_2 at the bridge site as the FS. The reaction barrier for this step is 2.38 eV, and the corresponding reaction energy is endothermic by 0.67 eV.

CH_3NH decomposition. Comparatively, CH_3NH_2 decomposition prefers to through the initial N–H path to form the CH_3NH intermediate and the H atom. Once CH_3NH is formed, it can further dehydrogenate to produce CH_2NH and/or CH_3N, or to yield CH_3 and NH through the C–N bond scission.[25]

$CH_3NH \rightarrow CH_2NH + H$. The C–H bond activation begins with CH_3NH at the top site. In the TS4, CH_2NH locates at the hcp site with η^2(N)–η^1(C) configuration and the departed H atom locates at the bridge site. The activated C–H bond is lengthened to 1.516 Å. After the TS4, H moves to the top site while CH_2NH remains at the hcp site, forming the FS. The reaction energy for this step is slightly endothermic by 0.21 eV with an energy barrier of 1.28 eV.

$CH_3NH \rightarrow CH_3N + H$. The N–H bond scission in CH_3NH produces CH_3N and atomic H. In the TS5, CH_3N locates at the bridge site with η^2(N) configuration and the H atom locates at the top site, while the activated N–H bond is lengthened to 2.526 Å. In the FS, CH_3N locates at the bridge site and atomic H at the top site. This step is endothermic by 1.09 eV, and the energy barrier is 1.19 eV.

$CH_3NH \rightarrow CH_3 + NH$. Similar to CH_3NH_2, the C–N bond of CH_3NH is activated by virtue of the C–N bond stretching vibration, yielding an adsorbed CH_3 at the top site and NH at the fcc site. In the TS6, CH_3 locates at the top site and NH at the bridge site, the relevant C–N distance is calculated to be 2.116 Å. This step is unfavorable due to the high energy barrier of 2.27 eV encountered, and it is endothermic by 0.19 eV.

CH_2NH decomposition. CH_2NH is one product of CH_3NH decomposition *via* the C–H bond scission, and/or CH_2NH_2 decomposition *via* the N–H bond scission (see ESI†). It can be envisioned that further CH_2NH decomposition may also involve the C–H, N–H and C–N bond scissions.

$CH_2NH \rightarrow HCNH + H$. For further C–H bond scission, the IS CH_2NH locates at the fcc site with η^2(N)–η^1(C) configuration. One of the methylene H atoms wiggles along the C–N axis to the surface, yielding HCNH at the bridge site and H atom at the top site. In the TS8, HCNH tilts on the bridge site and H atom locates at the hcp site, the relevant C–H distance is elongated to 1.435 Å from 1.098 Å in the IS. This dehydrogenation *via* the C–H bond activation leads to a slightly endothermic reaction with an activation barrier of 1.31 eV.

$CH_2NH \rightarrow CH_2N + H$. The N–H bond scission in CH_2NH produces CH_2N and atomic H. In the TS9, CH_2N locates at the fcc site and H at the hcp site, the N–H and H–Pt distances are 1.408 and 1.789 Å, respectively. After the TS, CH_2N remains at the fcc site with the N–Pt distance further shortened to 2.076 Å and 2.082 Å, and H moves to the adjacent top site. This step has an energy barrier of 1.38 eV and reaction energy of 0.66 eV.

$CH_2NH \rightarrow CH_2 + NH$. The C–N bond cleavage in CH_2NH is activated by virtue of the C–N bond stretching vibration, producing CH_2 and NH. In the TS10, CH_2 sits at the top site and NH at the bridge site, and the C–N distance is 2.287 Å. Following the TS, CH_2 moves towards the bridge site and NH to the fcc site, forming the FS. The activation barrier for the reaction to CH_2 + NH reaches up to 2.47 eV and the reaction energy amounts to 0.94 eV, suggesting this elementary step is energetically unfeasible.

CH_3N decomposition. Further reaction of CH_3N involves two possibilities, that is, the C–H and C–N bond scissions.

$CH_3N \rightarrow CH_2N + H$. The C–H bond scission starts with CH_3N at the fcc site as the IS, ends with CH_2N binding upright at the bridge site *via* η^2(N) configuration and the atomic H at the top site as the FS. In the TS11, CH_2N remains at the initial site and the atomic H moves to the hcp site, and the relevant C–H bond length is elongated to 1.683 Å. The calculated energy barrier of this step is 1.71 eV, and the reaction energy is 0.62 eV.

$CH_3N \rightarrow CH_3 + N$. The C–N bond scission of CH_3N leads to the CH_3 and atomic N. In the TS12, CH_3 locates at the hcp site and N remains at the fcc site; the relevant C–N distance is elongated to 2.395 Å (1.451 Å in the IS). In the FS, CH_3 locates at the top site and the atomic N still at the fcc site. The energy barrier of this step is 2.64 eV, and the reaction energy is endothermic by 0.69 eV.

CH_2N decomposition. CH_2N is one of the products of CH_2NH decomposition *via* the N–H bond scission and/or CH_3N decomposition *via* the C–H bond scission, and the CH_2N decomposition may involve further C–H and C–N bond scissions.

$CH_2N \rightarrow HCN + H$. Further decomposition of CH_2N would lead to HCN and the atomic H. In the TS13, both HCN and the atomic H locate at the bridge site, with the C–H distance is elongated to 1.255 Å. After the TS, HCN moves to the bridge site with η^1(N)–η^1(C) configuration, and the atomic H moves towards an adjacent top site. This step is exothermic by 0.11 eV with an energy barrier of 0.82 eV.

$CH_2N \rightarrow CH_2 + N$. The C–N bond scission starts with CH_2N at the fcc site with η^2(N)–η^1(C) configuration, ends with CH_2 at the neighboring bridge site and N at the initial fcc site. In the TS14, CH_2 moves to the off-top site and N to the fcc site, the relevant C–N distance is 1.938 Å. This step accounts for an energy barrier of 2.04 eV with a corresponding reaction energy of 1.10 eV.

HCNH decomposition. Once HCNH is formed, it can undergo subsequent dehydrogenation to stably produce HCN through the N–H bond scission. In the TS15, HCN remains at the initial bridge site and the atomic H moves towards the adjacent off-bridge site with the N–H distance of 1.346 Å. After the TS, HCN remains at the bridge site with η^1(N)–η^1(C) configuration, and the atomic H moves to the adjacent bridge site. This reaction proceeds with a barrier of 1.52 eV, and is endothermic by 0.65 eV. In addition, HCN would be possible to further decompose to form CN and H, or CH and N through the C–H or C–N bond scissions (see ESI†). However, HCN would rather escape from the surface than further decomposition according to our results.

Discussion

Competition of the initial bond scission

To provide further original insight into the energy barrier for the competition of CH_3NH_2 to HCN on Pt(111) *via* the initial C–H, N–H and C–N bond scissions, the energy barrier analysis and electronic structure analysis are presented in this section.

Energy barrier analysis. We decompose the calculated barrier E_a using the following formula:[45–47]

$$E_a = \Delta E_{sub} + \Delta E_{AB}^{def} + E_{AB}^{IS} + E_{int}^{TS} - E_A^{TS} - E_B^{TS} \quad (4)$$

where ΔE_{sub} measures the influence of the structural change of the substrate from IS to TS on the barrier ($\Delta E_{sub} = E_{sub}^{TS} - E_{sub}^{IS}$); ΔE_{AB}^{def} is the deformation energy, reflecting the effect of the structural deformation of AB on E_a; E_{AB}^{IS} is the adsorption energy of AB in the IS; E_{int}^{TS} is the interaction between A and B at the TS. E_A^{TS} (E_B^{TS}) is the binding energy of A(B) at the TS geometry without B(A); obviously, the former four terms contribute positively to E_a, while they have a reverse effect for the last two factors. As shown in Table 3, ΔE_{sub} values show a slight fluctuation from 0.06 to 0.10 eV, indicating that the structural changes of the substrate originated from the change of adsorbates having a slight effect on E_a. The adsorption energies of H in the TS (E_B^{TS}) change slightly for the C–H and N–H bond scissions (2.70 *vs.* 2.80 eV) due to the insensitivity of H at different sites. The value of $\Delta E_{AB}^{def} + E_{int}^{TS}$ is 4.27, 4.58 and 4.35 eV for the C–H, N–H and C–N bond scissions, respectively. These small fluctuations (~0.30 eV) among these three competitive steps indicate that the influence from intra-methylamine has a slight effect on the energy barrier. Consequently, the binding energies of the adsorbed fragment $E_A^{TS} + E_B^{TS}$, determine the difference of E_a between these three competitive steps. The values of $E_A^{TS} + E_B^{TS}$ decrease in the sequence of N–H (4.62 eV) > C–H (4.02 eV) > C–N (3.06 eV), corresponding to the energy barrier E_a in the sequence of N–H < C–H < C–N. This is similar to the previous studies of initial CH_3NH_2 decomposition on Ni(100) and Ni(111).[24] In brief, the binding energy of the adsorbed fragment plays a crucial role in the energy barrier of the initial CH_3NH_2 decomposition on Pt(111), and thus determines which initial scission is more facile, the C–H, N–H or C–N bond scission.

Table 3 Energy barrier and contribution factors (in eV) for the initial bond scissions of methylamine decomposition on Pt(111)

Reaction	ΔE_{sub}	ΔE_{AB}^{def}	E_{AB}^{IS}	E_{int}^{TS}	E_A^{TS}	E_B^{TS}	E_a
(a) $CH_3NH_2 \rightarrow CH_2NH_2 + H$	0.06	3.23	0.99	1.04	1.32	2.70	1.30
(b) $CH_3NH_2 \rightarrow CH_3NH + H$	0.10	4.02	0.99	0.56	1.82	2.80	1.05
(c) $CH_3NH_2 \rightarrow CH_3 + NH_2$	0.09	2.96	0.99	1.39	1.03	2.03	2.38

Electronic structure analysis. We demonstrate the density of states projected onto the *d*-states (d-PDOS) of surface Pt atoms on the bare surface and TS. Fig. 4 shows the Δd-PDOS of surface Pt atoms by subtracting d-PDOS of the bare surface from that of TS for the C–H, N–H and C–N bond scissions of CH_3NH_2 decomposition on Pt(111). Quantitatively, the stabilization energy (E_d) of the d-states is calculated using the following equation:[24,47,48]

$$E_d = \int_{-\infty}^{E_F} \varepsilon\left(n_d^{TS} - n_d^{bare}\right) d\varepsilon \quad (5)$$

where n_d is the normalized density of states of Pt (electron per eV) with and without bonds to the TS adsorbates, and ε is the energy level. Generally, a larger absolute value of E_d means a

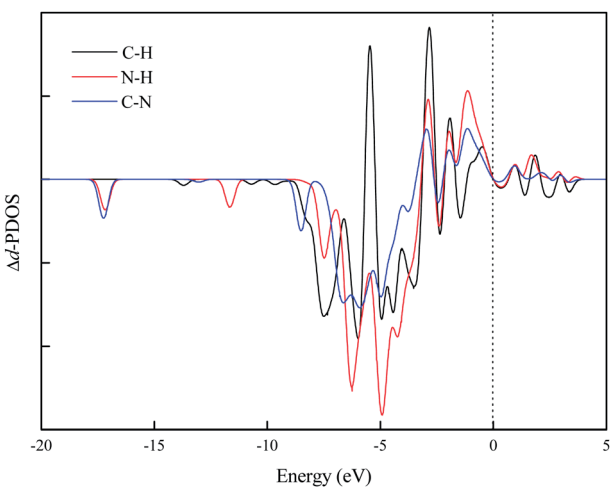

Fig. 4 Variation of the d-projected density of states of the surface Pt atom due to its bonding with TS complex in the initial C–H, N–H and C–N bond scissions of methylamine decomposition on Pt(111).

stronger interaction between the adsorbates and the surface, resulting in a lower activation energy. Here, the E_d value is calculated to be −8.52, −11.22 and −7.26 eV for the C–H, N–H and C–N bond scissions on Pt(111), respectively. This indicates that the interaction between the fragment and surface in the N–H bond scission is much stronger than that in the C–H and C–N bond scissions, in good agreement with the energy barrier decomposition analysis in Table 2.

Potential energy surfaces (PESs) and reaction mechanisms

The detailed PESs are presented in Fig. 5. In order to deeply understand the decomposition process, the rate constant k at 300 K is calculated for all elementary reactions involved in the decomposition processes (see Table 2).

The initial decomposition step of CH_3NH_2 prefers to take place *via* the N–H bond scission (reaction (b)) to form CH_3NH and H atom, and the C–H bond scission (reaction (a)) could serve as the alternative pathway due to the comparable energy barrier of 1.30 eV, agreeing well with the experimental result of CH_3NH_2 decomposition on Pt.[11] The most unfavorable pathway is the C–N bond scission (reaction (c)) because of the high energy barrier of 2.38 eV encountered. On the other hand, all energy barriers of CH_3NH_2 decomposition *via* the initial C–H, N–H and C–N bond scissions are larger than the desorption energy of 0.99 eV, indicating that desorption rather than decomposition would be preferable for adsorbed CH_3NH_2. The relevant rate constant of reactions (a), (b) and (c) at 300 K are calculated to be 9.59×10^{-1}, 1.11×10^{0} and 5.76×10^{-23} s^{-1}, respectively. For the successive decomposition reactions, the CH_3NH fragment is not kinetically facile to decompose *via* the C–N bond scission (reaction (f)), while those *via* the C–H and/or N–H bond scissions might take place owing to their relatively low energy barriers of 1.28 and 1.19 eV along reactions (d) and (e). As for the relevant rate constant of reactions (d) and (e) at 300 K, they are in the same order of magnitude, 1.98×10^{-3} and 2.27×10^{-3} s^{-1}, identifying both the C–H and N–H bond scissions as parallel routes for CH_3NH decomposition. Analogously, the C–N bond scission (reaction (j)) is unfavorable for CH_2NH decomposition due to the high energy barrier of 2.47 eV encountered, while the C–H and/or N–H bond scissions (reaction (h) and (i)) have comparable energy barriers of 1.31 and 1.38 eV. The relevant rate constants at 300 K are 4.17×10^{-2} and 4.96×10^{-4} s^{-1}, respectively. For CH_3N, the C–H bond scission (reaction (k)) to CH_2N occurs with an energy barrier of 1.71 eV, which is much lower than the C–N bond scission (reaction (l)) to CH_3 and N atom. Similarly, the rate constant of the C–H bond scission (reaction (m)) is twenty-five orders of magnitude greater than that of C–N bond (reaction (n)), suggesting much greater facility for the scission of the C–H bond in CH_2N than that of the C–N bond. In brief, the PESs and rate constant analysis show that the direct C–N bond scission is unfavorable for decomposition of CH_3NH_2 and its C, N-containing intermediates, while the C–H and/or N–H bond scissions stay competitive on all intermediates decompositions. Comparatively, the most favorable reaction pathway proceeds *via* $CH_3NH_2 \rightarrow CH_3NH \rightarrow CH_3N \rightarrow CH_2N \rightarrow HCN$, testifying the experimental speculation of the reaction processes ($CH_3NH_2 \rightarrow CH_3NH \rightarrow CH_2N \rightarrow HCN$).[11]

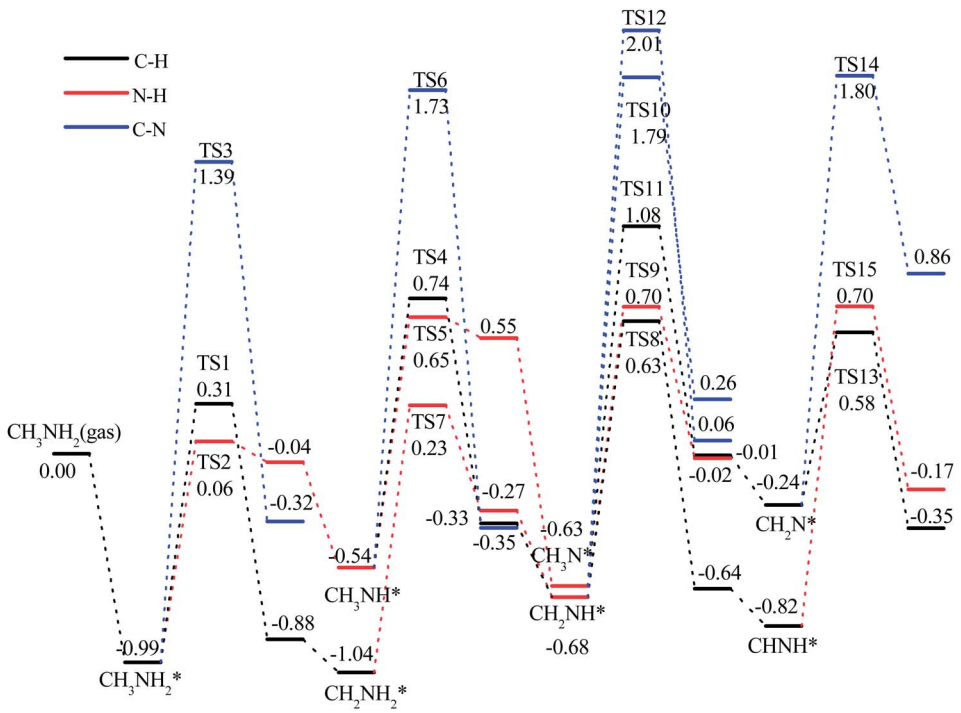

Fig. 5 Potential energy surfaces (PES) of methylamine decomposing to HCN on Pt(111). The energy reference corresponds to the total energy of one methylamine molecule and the clean slab. The black line represents the C–H bond scission path, while the red and blue indicate N–H and C–N bond scission pathway, respectively.

Brønsted–Evans–Polanyi (BEP) relations

In order to further distinguish the selectivity of bond scission, we make a comparison of the energy barrier and the reaction energy, known as the BEP behavior,[49,50] for each elementary step. The elementary reactions are written as exothermic steps, and the IS and FS are defined accordingly.[51] The energy reference for each step is the clean slab plus gas-phase energy of the corresponding reactants. As shown in Fig. 6, we can identify three distinct beelines for the C–H, N–H and C–N bond scissions reactions. This feature reflects that no single BEP relation can be established for all reactions on the same surface, whereas in each bond scission class, a linear BEP relationship holds roughly for most reactions. The black line represents the C–H bond scission, the linear regression equation is $E_{TS} = 0.83\ E_{FS} + 0.97$ (eV), the square of the correlation coefficient is 0.92, and the standard error is 0.27; the red line represents the N–H bond scission, the linear regression equation is $E_{TS} = 0.88\ E_{FS} + 1.05$ (eV), the square of the correlation coefficient is 0.96, and the standard error is 0.16; the blue line represents the C–N bond scission, the linear regression equation is $E_{TS} = 0.92\ E_{FS} + 2.22$ (eV) with the square of the correlation coefficient and the standard error is 0.95 and 0.25, respectively. As shown in Fig. 6, the beelines of the C–H, N–H and C–N bond scissions are almost parallel while the intercept of the C–N bond scission is obviously larger than the others. This means that the C–N bond scission is quite unfavourable to take place with respect to the C–H and N–H bond scissions. Both beelines of the C–H and N–H bonds are close to each other and appear a cross point, indicating that there is intense competition between the C–H and N–H bond scissions for CH_3NH_2 and its C, N-containing intermediate decomposition.

It can be found that two points deviate from the lines obviously, *e.g.*, points 1 and 2. Point 1 corresponds to the only exothermic C–H bond scission in $CH_2N \rightarrow HCN + H$ as shown in Table 2, resulting from the stable FS and relatively low energy barrier. Point 2 corresponds to the C–N bond scission of CH_2N, and the obvious corrugation of the metal surface destabilizes the TS (see Fig. 2 TS14) and thus decreases the energy barrier. Checking the structures involved in all reactions, it is interesting to note that, unlike other steps, the TS structures corresponding to these deviated points do not resemble the FS structures, in good agreement with the previous results that the surface reaction following the general BEP principle possesses a TS.[50,51] Besides, the BEP relationship can be used as a convenient approach to determine the most likely dissociation sites and kinetic data based on the thermodynamic parameters for reactions occurring on the surface.[52]

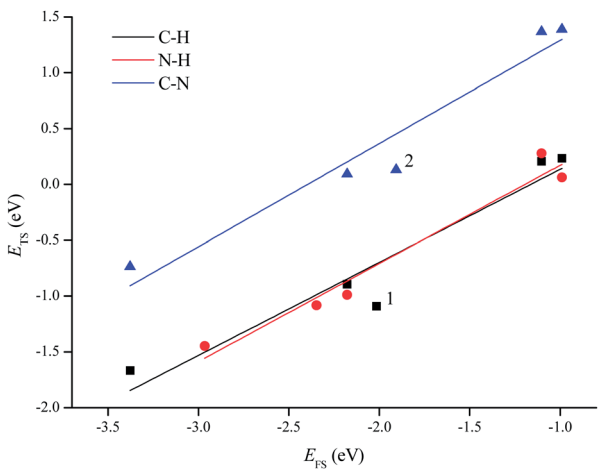

Fig. 6 Plot of the TS energy against the FS energy for all bond scission reactions involved in methylamine decomposing to HCN on Pt(111). The square, circle and triangle symbols denote the C–H, N–H and C–N bond breaking reactions, respectively. The points with the largest deviation correspond to reactions $CH_2N \rightarrow HCN + H$ (labelled as 1) and $CH_2N \rightarrow CH_2 + N$ (labelled as 2).

Conclusions

Our DFT investigation provides a systematic understanding of the decomposition mechanism of CH_3NH_2 to HCN on Pt(111) and a deep insight into the selectivity of the C–H, N–H and C–N bond scissions. Our results show that CH_3NH_2 weakly adsorbs on the Pt surface *via* the lone pair electron of the N atom and prefers desorption to decomposition. The C–H and/or N–H bond scissions stay competitive in all elementary steps involved, but the C–N bond scission is not facile to take place. The most favourable reaction pathway proceeds *via* $CH_3NH_2 \rightarrow CH_3NH \rightarrow CH_3N \rightarrow CH_2N \rightarrow HCN$. The interaction between the fragments and the surface in the TS plays a decisive role in controlling the energy barrier E_a of CH_3NH_2 decomposition *via* the initial C–H, N–H and C–N bond scissions on Pt(111). BEP analysis identifies that the C–H and N–H bond scissions stay competitive, but the C–N bond scission is not facile to take place.

Acknowledgements

This work was supported by NSFC (21303266), Shandong Province Natural Science Foundation (ZR2011EMZ002), PetroChina Innovation Foundation (2013D-5006-0406), the Fundamental Research Funds for the Central Universities (13CX02001A, 13CX05020A), the Promotive Research Fund for Excellent Young and Middle-aged Scientists of Shandong Province (BS2013CL031), and the Graduate Innovative Foundation of China University of Petroleum (CX-1251, CX2013023).

References

1 A. G. Baca, M. A. Schulz and D. A. Shirley, *J. Chem. Phys.*, 1985, **83**, 6001–6008.
2 S. Y. Hwang, E. G. Seebauer and L. D. Schmidt, *Surf. Sci.*, 1987, **188**, 219–234.
3 A. J. Hernández-Maldonado and R. T. Yang, *Angew. Chem., Int. Ed.*, 2004, **43**, 1004–1006.
4 G. A. Cordonier, F. Schüth and L. D. Schmidt, *Vacuum*, 1990, **41**, 278–281.
5 D. Hasenberg and L. D. Schmidt, *J. Catal.*, 1986, **97**, 156–168.
6 V. A. Kondratenko, *Appl. Catal., A - Gen.*, 2010, **381**, 74–82.

7 L. D. Schmidt and D. A. Hickman, *Catalysis of Organic Reactions*, Taylor & Francis, New York, 1994.
8 T. S. Nunney, J. J. Birtill and R. Raval, *Surf. Sci.*, 1999, **427–428**, 282–287.
9 G. R. Schoofs and J. B. Benziger, *J. Phys. Chem.*, 1988, **92**, 741–750.
10 D. E. Gardin and G. A. Somorjai, *J. Phys. Chem.*, 1992, **96**, 9424–9431.
11 M. E. Bridge and J. Somers, *Vacuum*, 1988, **38**, 317–320.
12 S. Y. Hwang and L. D. Schmidt, *J. Catal.*, 1988, **114**, 230–245.
13 D. Jentz, M. Trenary, X. D. Peng and P. Stair, *Surf. Sci.*, 1995, **341**, 282–294.
14 P. A. Thomas and R. I. Masel, *J. Vac. Sci. Technol., A*, 1987, **5**, 1106–1108.
15 S. Y. Hwang, A. C. F. Kong and L. D. Schmidt, *J. Phys. Chem.*, 1989, **93**, 8327–8333.
16 J. J. Chen and N. Winograd, *Surf. Sci.*, 1995, **326**, 285–300.
17 F. Maseri, A. Peremans, J. Darville and J. M. Gilles, *J. Electron Spectrosc. Relat. Phenom.*, 1990, **54–55**, 1059–1064.
18 K. A. Pearlstine and C. M. Friend, *J. Am. Chem. Soc.*, 1986, **108**, 5842–5847.
19 R. Bafrali and A. T. Bell, *Surf. Sci.*, 1992, **278**, 353–363.
20 D. F. Johnson, Y. Wang, J. E. Parmeter, M. M. Hills and W. H. Weinberg, *J. Am. Chem. Soc.*, 1992, **114**, 4279–4290.
21 T. Kato, S.-Y. Kang, X. Xu and T. Yamabe, *J. Phys. Chem. B*, 2001, **105**, 10340–10347.
22 J.-H. Cho and L. Kleinman, *Phys. Rev. B: Condens. Matter Mater. Phys.*, 2003, **67**, 201301.
23 X. Q. Lu, W. Y. Guo, L. M. Zhao, X. F. Chen, Q. T. Fu and Y. Ma, *J. Organomet. Chem.*, 2007, **692**, 3796–3803.
24 C. Q. Lv, J. Li, K. C. Ling, Z. F. Shang and G.-C. Wang, *Surf. Sci.*, 2010, **604**, 779–787.
25 C. Q. Lv, J. H. Liu, Y. Guo and G. C. Wang, *Phys. Chem. Chem. Phys.*, 2012, **14**, 6869–6882.
26 J. H. Liu, C. Q. Lv, D. L. Du and Y. Guo, *J. Nat. Gas Chem.*, 2012, **21**, 132–137.
27 J. H. Liu, C. Q. Lv, Y. Guo and G. C. Wang, *Appl. Surf. Sci.*, 2013, **271**, 291–298.
28 C. Oliva, C. van den Berg, J. W. Niemantsverdriet and D. Curulla-Ferré, *J. Catal.*, 2007, **245**, 436–445.
29 C. Oliva, C. van den Berg, J. W. Niemantsverdriet and D. Curulla-Ferré, *J. Catal.*, 2007, **248**, 38–45.
30 D. Hasenberg and L. D. Schmidt, *J. Catal.*, 1987, **104**, 441–453.
31 S. Delagrange and Y. Schuurman, *Catal. Today*, 2007, **121**, 204–209.
32 H. Y. Zhu, W. Y. Guo, R. B. Jiang, L. M. Zhao, X. Q. Lu, M. Li, D. L. Fu and H. H. Shan, *Langmuir*, 2010, **26**, 12017–12025.
33 B. Delley, *J. Chem. Phys.*, 1990, **92**, 508–517.
34 B. Delley, *J. Chem. Phys.*, 1996, **100**, 6107–6110.
35 B. Delley, *J. Chem. Phys.*, 2000, **113**, 7756–7764.
36 J. P. Perdew, *Phys. Rev. B: Condens. Matter Mater. Phys.*, 1986, **33**, 8822–8824.
37 J. P. Perdew and Y. Wang, *Phys. Rev. B: Condens. Matter Mater. Phys.*, 1992, **45**, 13244–13249.
38 J. P. Perdew, K. Burke and M. Ernzerhof, *Phys. Rev Lett.*, 1996, **77**, 3865–3868.
39 B. Delley, *Phys. Rev. B: Condens. Matter Mater. Phys.*, 2002, **66**, 155125–155133.
40 H. J. Monkhorst and J. D. Pack, *Phys. Rev. B: Solid State*, 1976, **13**, 5188–5192.
41 T. A. Halgren and W. N. Lipscomb, *Chem. Phys. Lett.*, 1977, **49**, 225–232.
42 W. F. K. Wynne-Jones and H. Eyring, *J. Chem. Phys.*, 1935, **3**, 492–502.
43 W. K. Offermans, A. P. J. Jansen and R. A. van Santen, *Surf. Sci.*, 2006, **600**, 1714–1734.
44 X. Q. Lu, L. Liu, Y. Li, W. Y. Guo, L. M. Zhao and H. H. Shan, *Phys. Chem. Chem. Phys.*, 2012, **14**, 5642–5650.
45 Y. L. Cao and Z. X. Chen, *Phys. Chem. Chem. Phys.*, 2007, **9**, 739–746.
46 X. Q. Lu, Z. G. Deng, K. S. Chau, L. F. Li, Z. Q. Wen, W. Y. Guo and C. M. L. Wu, *ChemCatChem*, 2013, **5**, 1832–1841.
47 Z. G. Deng, X. Q. Lu, Z. Q. Wen, S. X. Wei, Y. J. Liu, D. L. Fu, L. M. Zhao and W. Y. Guo, *Phys. Chem. Chem. Phys.*, 2013, **15**, 16172–16182.
48 H. F. Wang and Z. P. Liu, *J. Am. Chem. Soc.*, 2008, **130**, 10996–11004.
49 J. K. Nørskov, T. Bligaard, A. Logadottir, S. Bahn, L. B. Hansen, M. Bollinger, H. Bengaard, B. Hammer, Z. Sljivancanin, M. Mavrikakis, Y. Xu, S. Dahl and C. J. H. Jacobsen, *J. Catal.*, 2002, **209**, 275–278.
50 M. Li, W. Y. Guo, R. B. Jiang, L. M. Zhao and H. H. Shan, *Langmuir*, 2010, **26**, 1879–1888.
51 R. Alcalá, M. Mavrikakis and J. A. Dumesic, *J. Catal.*, 2003, **218**, 178–190.
52 W. Y. Guo, M. Li, X. Q. Lu, H. Y. Zhu, Y. Li, S. R. Li and L. M. Zhao, *Dalton Trans.*, 2013, **42**, 2309–2318.